Low Temperature Physics/Fizika Nizkikh Temperatur, 2020, v. 46, No. 8, pp. 1021–1027

Non-uniform along thickness spin excitations in magnetic vortex-state nanodots

G.N. Kakazei

Institute of Physics for Advanced Materials, Nanotechnology and Photonics (IFIMUP)
Departamento de Física e Astronomia, Universidade do Porto, Porto 4169-007, Portugal
E-mail: gleb.kakazei@fc.up.pt

K.Y. Guslienko

Departamento de Física de Materiales, Universidad del País Vasco, San Sebastián 20018, Spain
IKERBASQUE, the Basque Foundation for Science, Bilbao 48011, Spain

R.V. Verba

Institute of Magnetism NAS of Ukraine and MES of Ukraine, Kyiv 03142, Ukraine

J. Ding, X.M. Liu, and A.O. Adeyeye*

Information Storage Materials Laboratory, Department of Electrical and Computer Engineering
National University of Singapore, Singapore 117576, Singapore

Received April 16, 2020, published online June 22, 2020

We summarize our experimental findings in the arrays of $Ni_{80}Fe_{20}$ circular nanodots with diameter 300 nm and thickness 20 nm $\le L \le$ 100 nm, probed by broadband ferromagnetic resonance spectroscopy in the absence of external magnetic field. Spin excitation modes related to the vortex core gyrotropic dynamics were observed in the gigahertz frequency range. Micromagnetic simulations revealed that they are flexure oscillations of the vortex core string with $n = 0, 1, 2$ nodes along the dot thickness. It was found that for $L > 70$ nm the intensity of more complicated $n = 1$ vortex gyrotropic mode is unexpectedly higher than the one of the lowest $n = 0$ gyrotropic mode. This behavior was clarified on the basis of the inhomogeneous vortex mode phase profiles extracted from micromagnetic simulations and calculated analytically. Precise measurements of the dependence of resonance frequency of the vortex $n = 0$ mode on the dot thickness demonstrated a clear maximum around $L = 70$ nm, that was theoretically explained by introducing a vortex mass, which is a result of the vortex distortion due to interaction with spin waves having azimuthal indices $m = \pm 1$. Finally, several azimuthal spin-wave modes having curled structure at the dot top and bottom faces were found in the spectrum of the dots with thicknesses $L \ge 40$ nm.

Keywords: nanodot, ferromagnetic resonance, spin excitations, vortex gyrotropic mode.

Introduction

Spin waves (SW) in ferromagnets were first introduced by Bloch [1] on the ground of microscopic approach. The phenomenological magnetization dynamics was described by Landau and Lifshitz by their classical equation of motion [2,3]. By the late 50th of 20th century the detailed theoretical analysis of spin waves has been performed in Refs. 4, 5. Finally, the spin waves in ferromagnetic films, predicted by Kittel in Ref. 5, were observed experimentally in 1958 [6]. This initial stage of the investigation of spin waves has been summarized in the review articles [7,8] and, later, in the classical monograph by Akhiezer, Bar'yakhtar and Peletminski [9]. With the development of patterning techniques, particularly electron-beam lithography, standing SW modes were observed in thin micron and submicron sized ferromagnetic elements due to their confined geometry [10–13]. Having in mind that the magnetic patterned nanoelements are being used in many real world applications — magnetic recording read-write heads [14], magnetic random access memories [15], and spin-torque nano-oscillators [16], just to name a few — it is crucial to know and understand their SW excitation spectra.

* Present address: Department of Physics, Durham University, South Rd, Durham, DH1 3LE, UK

It is well known that submicron flat elements, made of soft ferromagnetic materials, have a vortex state of magnetization as the ground state for certain relations between the element thicknesses and lateral sizes. This is a result of competition of exchange and magneto-dipolar energies [17]. Recently it was demonstrated that the vortex can be stabilized in ultrathin soft magnetic dots with diameter as small as 60 nm by exposing dot to strong magnetic field with radial symmetry [18]. Vortex state was experimentally observed by magnetic force microscopy [19]. It is characterized by in-plane curling magnetization configuration and a small (~10 nm) region of the vortex core with out-of-plane magnetization, see the review [20] and references therein. After prediction of the vortex gyrotropic mode in circular dots [21] in the form of the vortex core sub-GHz oscillations, this mode was observed by time-resolved Kerr microscopy [22]. Then, it was demonstrated in [23] using broadband ferromagnetic resonance (FMR) technique that the vortex gyrotropic mode can be excited by in-plane microwave field. The vast majority of the further vortex dynamics studies were focused on thin magnetic elements with thicknesses below 40 nm and only uniform across the thickness vortex excitation modes were observed.

The higher order vortex gyrotropic modes were considered by micromagnetic simulations of magnetization dynamics in thick circular dots [24] and rectangular prisms [25]. These modes were described as flexure oscillations of the vortex core string with $n = 0, 1, 2\ldots$ nodes along the dot thickness. It was suggested in Ref. 25 that the uniform ($n = 0$) gyrotropic mode should have the same phase through the whole element thickness, whereas for the $n = 1$ mode at the top and bottom dot faces, the core rotates in the same direction but with 180° phase shift, and for $n = 2$ mode the rotations on top and bottom faces are shifted by 180° with respect to rotation in the dot center. It is important to note that in the described case the net magnetization for mode $n = 1$ is equal to zero and this mode should have zero intensity in both micromagnetic simulations and FMR experiments assuming uniform in-plane excitation microwave magnetic field. The 1st order vortex gyrotropic mode simulated by Boust and Vukadinovic [24] has non-zero intensity (although smaller than the uniform gyrotropic mode), suggesting that mode phase profile does not follow the simple picture proposed in [24].

Here we summarize our experimental findings in the arrays of soft magnetic $Ni_{80}Fe_{20}$ circular nanodots with thicknesses varied from 20 to 100 nm, probed by broadband ferromagnetic resonance spectroscopy. Higher order vortex gyrotropic modes were observed and their phase profiles were studied in details using analytical calculations and micromagnetic simulations. Vortex mass was introduced to explain the peculiar thickness dependence of the main gyrotropic mode with the index $n = 0$. Finally, azimuthal spin-wave modes having curled structure at the dot top and bottom faces were found in thick circular magnetic dots.

Experimental details

Periodic arrays of circular $Ni_{80}Fe_{20}$ dots with diameter $d = 300$ nm and pitch $p = 620$ nm were fabricated on Si substrate over 4×4 mm area using deep ultraviolet lithography at 248 nm exposure wavelength followed by electron beam evaporation and lift-off process. The thickness L of the $Ni_{80}Fe_{20}$ dots was varied from 20 to 100 nm. A representative scanning electron microscopy micrograph of the 60 nm thick $Ni_{80}Fe_{20}$ dot array is shown in Fig. 1a. Despite of the relatively large aspect ratio $b = (2\times L)/d = 0.266$,

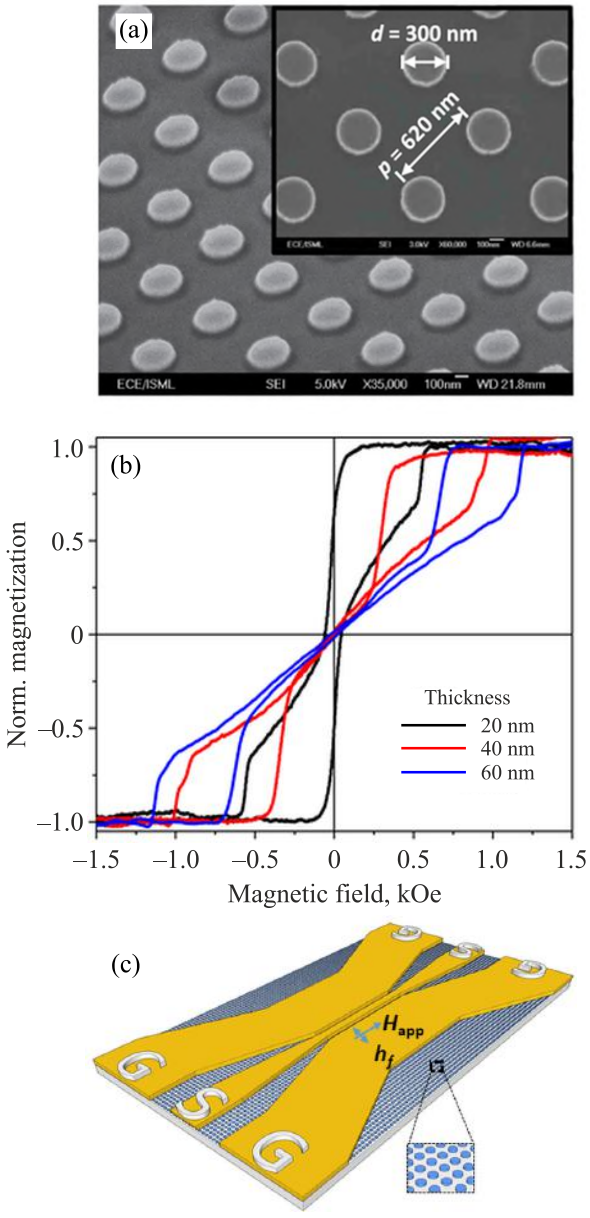

Fig. 1. (a) Scanning electron microscopy image (the viewing angle is 55°) of $Ni_{80}Fe_{20}$ dot array. The dot diameter $d = 300$ nm, pitch $p = 620$ nm and thickness $L = 60$ nm; (b) Hysteresis loops of the dots with different thicknesses measured by focused magneto-optical setup; (c) Experimental set-up for high frequency measurements of the dot arrays used for detection of the spin-wave excitation modes.

the dots are still looking like flat objects with sharp edges.

The magnetization behavior of the fabricated dot arrays was measured using focused magneto-optical Kerr setup with a spot size of about 5 μm in the longitudinal geometry (Fig. 1b). All the hysteresis loops have a double triangle shape and zero remanence, typical for the circular dots with the vortex ground state [20]. As expected, the vortex nucleation and annihilation fields became larger with dot thickness increase. These fields in all the samples are quite pronounced, which is a clear evidence of the dot's consistency inside the patterned arrays.

The microwave absorption of the samples was probed using a vector network analyzer by sweeping the frequency in 50 MHz − 20 GHz range in the absence of an external magnetic field at room temperature. The microwave field, h_f, is oscillating in the patterned film plane perpendicularly to the central waveguide. To maximize the sensitivity of microwave measurements, 50 Ohm coplanar waveguides with signal line length of 300 μm, width of 20 μm were fabricated on top of the dot arrays (Fig. 1c). The amplitude of the microwave magnetic field generated in the vicinity of the signal line was estimated to be ~2 Oe.

Results and discussion

The obtained experimental broadband microwave absorption spectra for different dot thicknesses L in the frequency range 50 MHz – 6 GHz are presented in the left panel of Fig. 2a. All the spectra contain two well-pronounced resonance peaks with quite different thickness dependence. The lower one is slightly shifting up from 0.8 to 1.0 GHz with initial thickness increase from $L = 50$ to 60 nm and with further thickness increase it returns back to 0.8 GHz for $L = 100$ nm. However, the frequency of the higher resonance peak is monotonically decreasing from 5.4 GHz for $L = 50$ nm to 2.4 GHz for 100 nm, i.e., by tuning the dot thickness in the 50–100 nm range, the frequency of the peak is reduced by 3 GHz. In addition, the relative intensity of the second peak drastically increases with the dot thickness increasing.

The identification of the experimentally observed peaks was performed using the LLG micromagnetic simulator [26]. Standard parameters for $Ni_{80}Fe_{20}$ alloy were used: the exchange stiffness constant $A = 1.05 \cdot 10^{-6}$ erg·cm^{-1}, gyromagnetic ratio $\gamma/2\pi = 2.93$ MHz/Oe and magnetic anisotropy constant $K_u = 0$. The values of saturation magnetization $M_s = 810$ emu/cm^3 and Gilbert damping parameter $\alpha = 0.01$ were extracted from FMR measurements on a reference 60 nm thick $Ni_{80}Fe_{20}$ continuous film. Cell size 5×5×5 nm was used in all micromagnetic simulations. The dot thicknesses were varied in the range 20–100 nm. For the case when the distance between dot centers is more than twice the dot diameter, the interdot dipolar interactions are considered to be negligible [27], therefore simulations were carried out for the individual dots. The simulated microwave absorption spectra for the dots with $d = 300$ nm and $L = 50$, 60, 80 and 100 nm are presented on the right panel of Fig. 2a. They demonstrate remarkable agreement with the experimental data. For simplicity of comparison, the intensities of both experimental and simulated spectra were normalized to the intensity of the strongest mode. Both the positions of two simulated low frequency peaks and their relative intensities are very similar to the experimental ones. Additionally, for $L = 80$ and 100 nm a third peak was observed at higher frequencies. Unfortunately, its intensity is significantly lower than intensity of two other peaks. Therefore it was not observed in our microwave experiments.

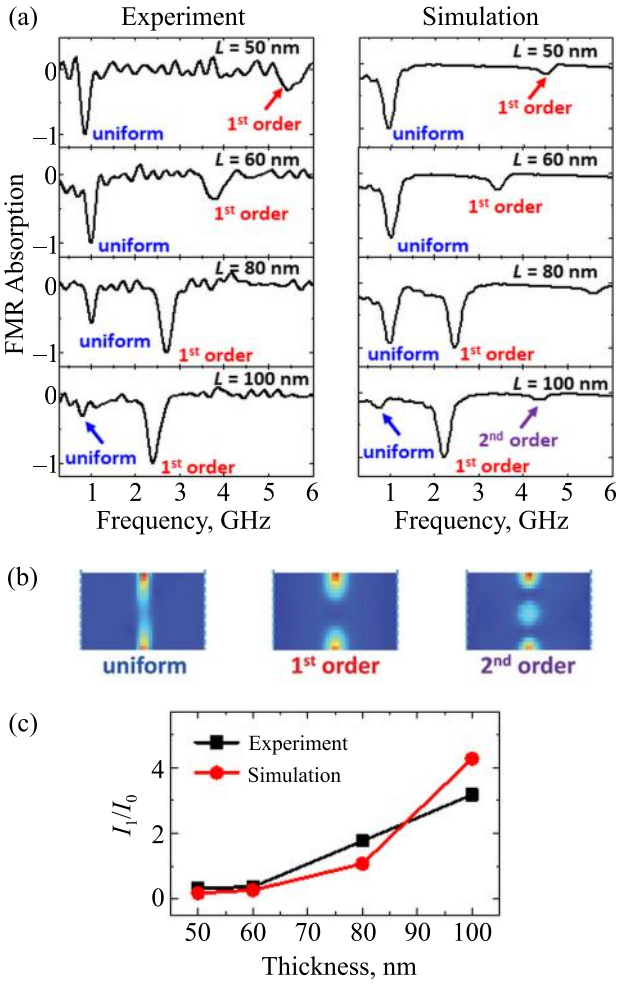

Fig. 2. (a) Experimental (left panel) and simulated (right panel) microwave absorption spectra in the absence of external magnetic field for the $Ni_{80}Fe_{20}$ circular dot arrays with different values of the dot thickness L varied from 50 to 100 nm; (b) Spatial distribution of three lowest eigen-modes for the dot with thickness $L = 100$ nm; (c) Dependence of the experimental and simulated relative mode I_1/I_0 intensity ratio on the dot thickness.

Figure 2b shows the spatial distribution of the magnetization along the excitation field direction of the three observed modes for the dot with $d = 300$ nm and $L = 100$ nm. These modes were excited by the sinusoidal microwave magnetic field with amplitude of 2 Oe, i.e., by the similar

field that was applied in the experiment. All the three modes correspond to the vortex core spin excitations. The lowest one is the almost uniform vortex gyrotropic mode, since it is excited in the whole thickness range from top to bottom, although its intensity depends a bit on thickness coordinate (no nodes, $n = 0$). The second mode has maximum intensity on upper and lower dot surfaces and is not excited in the dot center (one node, $n = 1$). Finally, the third mode has the maximum intensity on both the dot faces and in the dot center, with two unexcited areas lying in between (two nodes, $n = 2$). Therefore, the last two modes can be considered as the first and second resonances of the vortex core line or as high order gyrotropic vortex modes. This interpretation was confirmed by the analytical calculations conducted using Thiele equation of the vortex core motion in Ref. 28.

The most stunning feature of the 1th order vortex gyrotropic mode is the thickness dependence of the mode intensity — it increases with thickness and becomes more intensive than the uniform gyrotropic mode above $L = 70$ nm (Fig. 2c). To explain the observed anomalously high values of I_1/I_0 mode intensity ratio for thick dots we studied the phase profiles of the mentioned gyrotropic modes along dot thickness. For this purpose simulations with sine-wave excitations were performed. Excitations were applied at the frequencies previously determined as resonance frequencies of $n = 0$ and $n = 1$ modes from field pulse excitation simulations. The obtained results for both modes $n = 0, 1$ of the 100 nm thick dot are presented in Fig. 3. It was found that for all the samples in the dot middle cross-section the vortex core phase is always coincides with the phase of the driving magnetic field. At the dot top/bottom faces the phase can be shifted noticeably from its value at the central plane either clockwise or counterclockwise, and the phase profile is asymmetrical when compared with the dot middle-plane layer.

The simulated phase profiles of the mode $n = 0$ are presented on the left sides (and the ones of the mode $n = 1$ on the right sides) of the top panel of Fig. 3 for the dots with $L = 50$ nm and 100 nm. For the lowest-frequency vortex mode $n = 0$ in relatively thin dots ($L \leq 50$ nm) no phase shift was observed. However, with increase of the dot thickness, the phase difference between the dot top and bottom faces is increasing, reaching 127° for $L = 100$ nm. At the same time, the phase shift for the $n = 1$ mode decreases with thickness from ~100° at $L = 50$ nm to ~60° at $L = 100$ nm. Therefore, for the 100 nm thick dots the phase shift for the $n = 1$ mode is two times smaller than the one for the $n = 0$ mode. This can definitely explain the observed anomalous behaviour of the mode intensity I_1/I_0 ratio, since the effectiveness of mode interaction with external uniform microwave magnetic field determining the mode intensity decreases drastically with the phase shift increase [29].

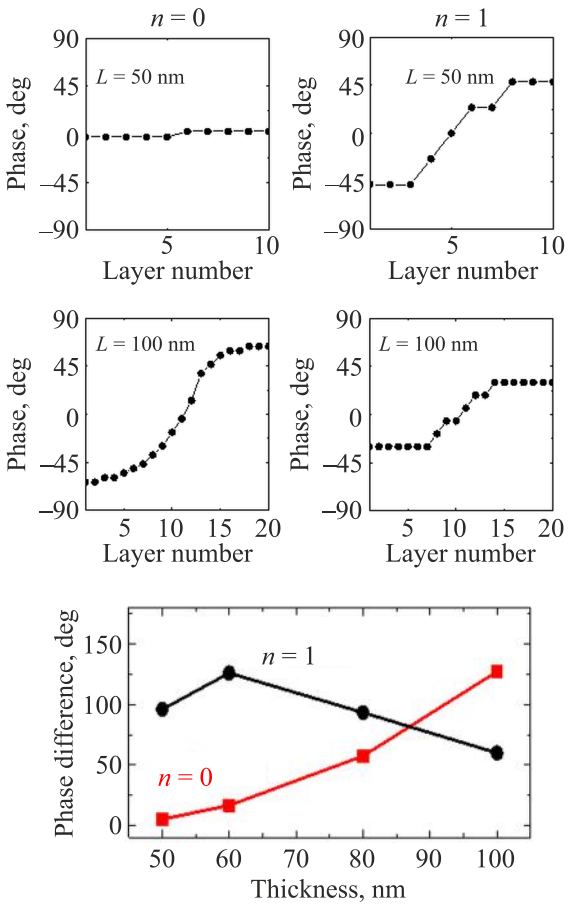

Fig. 3. Top panel: the phase profiles (obtained from micromagnetic simulations) of $n = 0$ (left) and $n = 1$ (right) vortex eigenmodes for 50 nm and 100 nm thick $Ni_{80}Fe_{20}$ dots, respectively. Bottom panel: phase difference between the vortex core position in the top and bottom layer for the 0th and 1th modes as a function of the dot thickness L.

It is interesting to note that the frequency of the lowest gyrotropic mode reveals a maximum as a function of the dot thickness (Fig. 4). The observed behavior can be explained on the basis of developed analytical theory [30], where the frequency of this mode was calculated by introducing an inertia (mass) term to the vortex equation of motion. Previously, the problem of vortex mass was discussed on the ground of numerical simulation of fast oscillations of the magnetic vortices, first, for discrete two-dimensional spin models [31,32] and, later, for thin circular magnetic particles [33,34]. In our case, the vortex mass appears due to a vortex interaction with azimuthal spin waves and is non-local due to the non-locality of the magnetostatic coupling. The vortex-SW interaction is linear in the vortex and SW amplitudes and is described by the concept of an emergent gauge field arising due to using of the moving coordinate frame related to the dynamic vortex magnetization [35]. The bilinear interaction is different from zero only for the spin waves having azimuthal indices $m = \pm 1$ ($2m$ is the number of nodes of the dynamical mag-

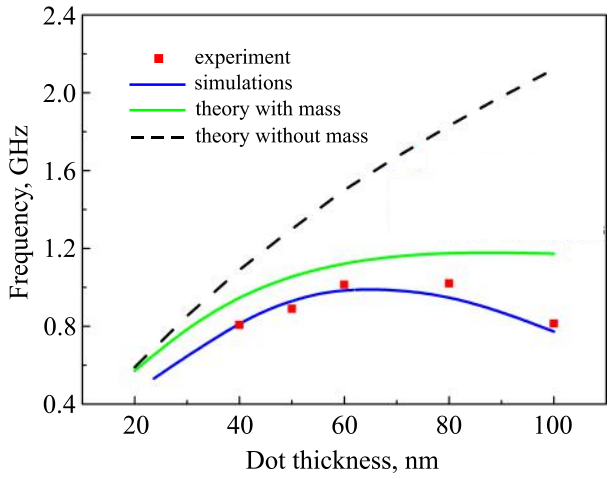

Fig. 4. (Color online) The frequency of the lowest vortex gyrotropic mode vs. dot thickness: red squares — the experimental data, blue solid line — the simulated frequencies, green solid line — the calculations according to Eq. (4) from Ref. 30 accounting the vortex mass, black dashed line — calculations without accounting for the vortex mass.

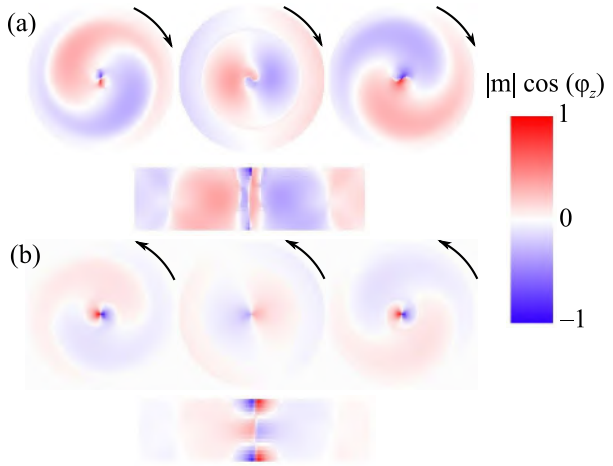

Fig. 5. (Color online) Normalized instant profiles at the top, central and bottom dot planes and cross-sections of the lowest clockwise (a) and counterclockwise (b) azimuthal modes for the circular magnetic dot with the thickness $L = 80$ nm; arrows show the direction of the mode "rotation".

netization in the azimuthal direction assuming a cylindrical coordinate system with the origin in the circular dot center). The introduced mechanism of magnetic vortex mass formation via interaction with the azimuthal spin waves is similar to appearance of the mass of some elementary particles via the Higgs mechanism (interaction with the Higgs field) [36]. In our case, the azimuthal magnons play a role of the Higgs bosons (excitations of the Higgs field). The magnetic vortex acquires a finite mass due to coupling with the magnons represented via a gauge field. This mass can be written in terms of the moving vortex mass within the generalized Thiele approach to the magnetic soliton motion. The vortex mass was found to increase nonlinearly with the dot thickness L and the calculated value of the vortex mass is approximately equal to a giant value order of 10^{-18} g for the dot thickness of 100 nm [30].

Finally, it was found that an increased magnetic dot thickness not only leads to the appearance of higher-order gyrotropic modes, but also modifies azimuthal spin-wave modes spectrum, where new "curled" spin-wave modes appear. These modes have characteristic curled structure at the top and bottom dot surfaces with opposite curling direction at them, and resemble common (l, $m = \pm 1$) azimuthal modes at the dot central plane (Fig. 5). Due to their complex magnetization configurations, the curled modes cannot be characterized by radial (l), azimuthal (m) and thickness (n) indices as all other spin-wave modes. Instead, they could be characterized by the number of radial nodes at the dot central plane. For the 80 nm thick circular dots up to third-order curled modes were observed.

The curled spin-wave modes originate from higher order thickness modes of the magnetic vortex-state dots and their appearance is directly related to the deviation of static magnetization configuration from quasi-two-dimensional with the dot thickness increase. The frequencies of the curled modes depend inversely on the dot thickness and, in particular, for thicknesses $L > 50$ nm they become the lowest among the azimuthal modes. Also, in contrast with common uniform along the dot thickness modes, the curled ones have a significant difference in the intensity between clockwise and counter-clockwise modes of the same type. Due to a complex non-uniform magnetization distribution, the curled modes have a small net magnetic moment, and, as a result, small excitation efficiency by uniform microwave magnetic field. For more details, please see [37].

Summary

The spin-wave excitation spectrum of thin (30 nm and below) circular ferromagnetic dots in the vortex state under in-plane excitation magnetic field consists of the uniform gyrotropic mode and doublets of azimuthal modes with different radial indices. With thickness increase the spectra became more complicated. First, the higher order vortex gyrotropic modes (flexure oscillations of the vortex core string with nodes along the dot thickness) become noticeable and their relative intensities grow with the thickness increase. Second, at higher frequencies new spin-wave modes having curled structure at the dot top/bottom dot surfaces and radial nodes at the dot central plane appear. Such complex magnetization configuration of the spin-wave modes is a consequence of increasing thickness nonuniformity of the effective magnetic field in thick dots. Finally, the vortex mass was introduced to explain the peculiar thickness dependence of the lowest vortex gyrotropic mode.

Acknowledgements

G.N.K. acknowledges the Network of Extreme Conditions Laboratories and Portuguese Foundation of Science and Technology (FCT) for support through Projects No. NORTE-01-0145-FEDER-022096, and No. POCI-0145-FEDER-030085 (NOVAMAG). K.Y.G. acknowledges the support from IKERBASQUE (the Basque Foundation for Science) and the Spanish Ministry of Economy, Industry and Competitiveness, Grant No. FIS2016-78591-C3-3-R. R.V.V. acknowledges the support by the Ministry of Education and Science of Ukraine, Project No. 0118U004007.

1. F. Bloch, *Z. Phys.* **61**, 206 (1930).
2. L.D. Landau and E.M. Lifshitz, *Phys. Z. Sowjet* **8**, 153 (1935).
3. E.M. Lifshitz, *Zh. Eksp. Teor. Fiz.* **15**, 1 (1945).
4. A.I. Akhiezer, V.G. Bar'yakhtar, and S.V. Peletminski, *Zh. Eksp. Teor. Fiz.* **35**, 474 (1958).
5. C. Kittel, *Phys. Rev.* **110**, 1295 (1958).
6. M.H. Seavey, Jr. and P.E. Tannenwald, *Phys. Rev. Lett.* **1**, 168 (1958).
7. A.I. Akhiezer, V.G. Bar'yakhtar, and M.I. Kaganov, *Usp. Fiz. Nauk* **71**, 533 (1960).
8. A.I. Akhiezer, V.G. Bar'yakhtar, and M.I. Kaganov, *Usp. Fiz. Nauk* **72**, 3 (1960).
9. A.I. Akhiezer, V.G. Bar'yakhtar, and S.V. Peletminski, *Spin Waves*, North-Holland, Amsterdam (1968).
10. J. Jorzick, S.O. Demokritov, C. Mathieu, B. Hillebrands, B. Bartenlian, C. Chappert, F. Rousseaux, and A.N. Slavin, *Phys. Rev. B* **60**, 15194 (1999).
11. G.N. Kakazei, P.E. Wigen, K.Y. Guslienko, V. Novosad, A.N. Slavin, V.O. Golub, N.A. Lesnik, and Y. Otani, *Appl. Phys. Lett.* **85**, 443 (2004).
12. G. de Loubens, A. Riegler, B. Pigeau, F. Lochner, F. Boust, K.Y. Guslienko, H. Hurdequint, L.W. Molenkamp, G. Schmidt, A.N. Slavin, V.S. Tiberkevich, N. Vukadinovic, and O. Klein, *Phys. Rev. Lett.* **102**, 177602 (2009).
13. G.N. Kakazei, G.R. Aranda, S.A. Bunyaev, V.O. Golub, E.V. Tartakovskaya, A.V. Chumak, A.A. Serga, B. Hillebrands, and K.Y. Guslienko, *Phys. Rev. B* **86**, 054419 (2012).
14. K. Tsunekawa, D.D. Djayaprawira, M. Nagai, H. Maehara, S. Yamagata, N. Watanabe, S. Yuasa, Y. Suzuki, and K. Ando, *Appl. Phys. Lett.* **87**, 072503 (2005).
15. S. Tehrani, B. Engel, J.M. Slaughter, E. Chen, M. DeHerrera, M. Durlam, P. Naji, R. Whig, J. Janesky, and J. Calder, *IEEE Trans. Magn.* **36**, 2752 (2000).
16. S.I. Kiselev, J.C. Sankey, I.N. Krivorotov, N.C. Emley, R.J. Schoelkopf, R.A. Buhrman, and D.C. Ralph, *Nature* **425**, 380 (2003).
17. R.P. Cowburn, A.O. Adeyeye, and M.E. Welland, *Phys. Rev. Lett.* **81**, 5414 (1998).
18. R.V. Verba, D. Navas, S.A. Bunyaev, A. Hierro-Rodriguez, B.A. Ivanov, K.Y. Guslienko, and G.N. Kakazei, *Phys. Rev. Appl.* **10**, 031002 (2018).
19. T. Shinjo, T. Okuno, R. Hassdorf, K. Shigeto, and T. Ono, *Science* **289**, 930 (2000).
20. K.Y. Guslienko, *J. Nanosci. Nanotechnol.* **8**, 2745 (2008).
21. K.Y. Guslienko, B.A. Ivanov, V. Novosad, Y. Otani, H. Shima, and K. Fukamichi, *J. Appl. Phys.* **91**, 8037 (2002).
22. J.P. Park, P. Eames, D.M. Engebretson, J. Berezovsky, and P.A. Crowell, *Phys. Rev. B* **67**, 020403 (2003).
23. V. Novosad, F.Y. Fradin, P.E. Roy, K.S. Buchanan, K.Y. Guslienko, and S.D. Bader, *Phys. Rev. B* **72**, 024455 (2005).
24. F. Boust and N. Vukadinovic, *Phys. Rev. B* **70**, 172408 (2004).
25. M. Yan, R. Hertel, and C.M. Schneider, *Phys. Rev. B* **76**, 094407 (2007).
26. M.R. Scheinfein, LLG Micromagnetics Simulator, Software for Micromagnetic Simulations, *http://llgmicro.home.mindspring.com* (1997).
27. G.N. Kakazei, Y.G. Pogorelov, M.D. Costa, T. Mewes, P.E. Wigen, P.C. Hammel, V.O. Golub, T. Okuno, and V. Novosad, *Phys. Rev. B* **74**, 060406 (2006).
28. J. Ding, G.N. Kakazei, X.M. Liu, K.Y. Guslienko, and A.O. Adeyeye, *Sci. Rep.* **4**, 4796 (2014).
29. J. Ding, G.N. Kakazei, X.M. Liu, K.Y. Guslienko, and A.O. Adeyeye, *Appl. Phys. Lett.* **104**, 192405 (2014).
30. K.Y. Guslienko, G.N. Kakazei, J. Ding, X.M. Liu, and A.O. Adeyeye, *Sci. Rep.* **5**, 13881 (2015).
31. G.M. Wysin, *Phys. Rev. B* **54**, 15156 (1996).
32. B.A. Ivanov, H.J. Schnitzer, F.G. Mertens, and G.M. Wysin, *Phys. Rev. B* **58**, 84861 (1998).
33. B.A. Ivanov, G.G. Avanesyan, A.V. Khvalkovskiy, N.E. Kulagin, C.E. Zaspel, and K.A. Zvezdin, *JETP Lett.* **91**, 178 (2010).
34. K.Y. Guslienko, G.R Aranda, and J. Gonzalez, *Phys. Rev. B* **81**, 014414 (2010).
35. K.Y. Guslienko, *EPL* **113**, 67002 (2016).
36. P.W. Higgs, *Phys. Rev.* **145**, 1156 (1966).
37. R.V. Verba, A. Hierro-Rodriguez, D. Navas, J. Ding, X.M. Liu, A.O. Adeyeye, K.Y. Guslienko, and G.N. Kakazei, *Phys. Rev. B* **93**, 214437 (2016).

Неоднорідні за товщиною спінові збудження магнітних нанодотів у вихровому стані

G.N. Kakazei, K.Y. Guslienko, R.V. Verba, J. Ding, X.M. Liu, A.O. Adeyeye

Підсумовано експериментальні результати у масивах круглих пермалоєвих нанодотів діаметром 300 нм і товщиною 20 нм $\le L \le$ 100 нм, досліджених методом широкосмугової феромагнітно-резонансної спектроскопії у відсутності зовнішнього магнітного поля. Моди спінового збудження, пов'язані з гіротропною динамікою ядра вихору, спостерігалися в гігагерцовому діапазоні частот. Мікромагнітне моделювання показало, що ці моди — коливання струни ядра вихору з $n = 0, 1, 2$ вузлами уздовж товщини нанодота. Виявлено, що для $L > 70$ нм інтенсивність гіротропної моди з $n = 1$ несподівано вище найнижчої гіротропної моди з $n = 0$. Така поведінка з'ясована на основі неоднорідних фазових профілей мод, отриманих з мікромагнітного моделювання і розрахованих аналітично.

Точні виміри залежності резонансної частоти найнижчої моди вихору з $n = 0$ від товщини нанодота показали існування максимуму в районі $L = 70$ нм, що було пояснено наявністю у вихорі маси, яка є результатом спотворення форми вихору внаслідок взаємодії зі спіновими хвилями, що мають азимутальні індекси $m = \pm 1$. Нарешті, у спектрі нанодотів з товщиною $L \geq 40$ нм виявлено кілька азимутальних спінхвильових мод, що мають скручену структуру на верхній та нижній гранях.

Ключові слова: нанодоти, феромагнітний резонанс, спінові збудження, вихровий гіротропний режим.